数理解析研究所講究録
第1890巻 2014年 149-159

Interaction between self-sustained flow oscillations and acoustic waves in a hole-tone system with an attached tailpipe

Mikael A. Langthjem† and Masami Nakano‡

†Graduate School of Science and Technology, Yamagata University,
Jonan 4-chome, Yonezawa-shi, 992-8510 Japan

‡Institute of Fluid Science, Tohoku University,
2-1-1 Katahira, Aoba-ku, Sendai-shi, 980-8577 Japan

Abstract

This paper is concerned with a mathematical model of a simple axisymmetric silencer-like model, consisting of a hole-tone feedback system equipped with by a tailpipe. The unstable shear layer is modeled via a discrete vortex method, based on axisymmetric vortex rings. The aeroacoustic model is based on the Powell-Howe theory of vortex sound. Boundary integrals are discretized via the boundary element method; but the tailpipe is represented by the exact (one-dimensional) solution. It is demonstrated though numerical examples that this numerical model can display lock-in of the self-sustained flow oscillations to the resonant acoustic oscillations.

1 Introduction

Expansion chambers are often used in connection with silencers in engine exhaust systems, with the aim of attenuating the energy flow. But the gas flow through the chamber may generate self-sustained oscillations, thus becoming a sound generator rather than a sound attenuator. Similar geometries and thus similar problems may be found in, for example, solid propellant rocket motors, valves, and heat exchangers.

The present work is related to a simple axisymmetric silencer model consisting of an expansion chamber followed by a tailpipe. The aim is to contribute to the understanding of the interaction between oscillations of the flow field and the acoustic field.

By oscillations of the flow field we mean the self-sustained oscillations of the jet shear layer. The shear layer is unstable and rolls up into a large, coherent vortex (a 'smoke-ring') which is convected downstream with the flow. It cannot pass through the hole in the downstream plate but hits the plate, where it creates a pressure disturbance. The disturbance is 'thrown' back (with the speed of sound) to the upstream plate, where it disturbs the shear layer. This initiates the roll-up of a new coherent vortex. In this way an acoustic feedback loop is formed, making up one type of flow-acoustic interaction.

These so-called hole-tone feedback oscillations may interact with the acoustic axial and radial eigen-oscillations of the cavity and the tailpipe. It is these interactions that we seek to understand. In the present paper we study the simplified configuration shown in Fig. 1. This is the hole-tone feedback system equipped with a tailpipe.

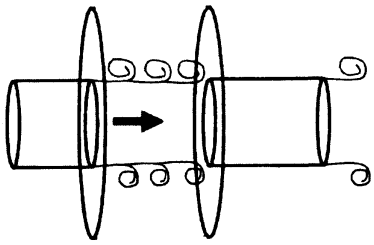

Figure 1: The hole-tone feedback system with a tailpipe. The arrow indicates the direction of the flow.

The unstable shear layer is modeled via a discrete vortex approach, based on axisymmetric vortex rings. The aeroacoustic model is based on the Powell-Howe theory of vortex sound [4, 5]. The boundary integrals that appear are discretized via the boundary element method.

The present paper concentrates on the aeroacoustic analysis. A description of the flow analysis (discrete vortex method) has been given in earlier papers [8, 9]. The geometry of the problem facilitates the use of cylindrical polar coordinates (r, θ, z), with the fluid flowing in the positive z-direction. Although it is possible that non-axisymmetric modes may be excited, we will, at this stage, consider only the axisymmetric modes (r, z).

The paper is organized as follows. The aeroacoustic model and its solution is described in Section 2. Section 3 considers details related to the boundary element discretization. The boundary element grid, and the representation of the tailpipe, is discussed in Section 4. Details regarding the solution of the tailpipe problem and the acoustic feedback model are discussed in Section 5. Numerical examples are given and discussed in Section 6. Finally, conclusions are given in Section 7.

2 Vortex sound

Modeling of the flow-induced sound is based on Howe's equation for vortex sound at low Mach numbers [4, 5]. Let $\mathbf{u}$ denote the flow velocity, $\boldsymbol{\omega} = \nabla \times \mathbf{u}$ the vorticity, c_0 the speed of sound, and ρ_0 the the mean fluid density. The sound pressure $p(\mathbf{x}, t)$ at the position $\mathbf{x} = (r, z)$ and time t is related to the vortex force (Lamb vector) $\mathfrak{L}(\mathbf{x}, t) = \boldsymbol{\omega}(\mathbf{x}, t) \times \mathbf{u}(\mathbf{x}, t)$ via the non-homogeneous wave equation

$$\left(\frac{1}{c_0^2} \frac{\partial^2}{\partial t^2} - \nabla^2 \right) p = \rho_0 \nabla \cdot \mathfrak{L}, \tag{1}$$

with boundary conditions $\partial p / \partial n = \nabla p \cdot \mathbf{n} = 0$ on the solid surfaces ($\mathbf{n}$ = normal vector), and $p \to 0$ for $|\mathbf{x}| \to \infty$.

To solve (1) and (2) in an axisymmetric setting, use is made of the free-space time-domain axisymmetric Green's function $G(t, \tau; r, z; r_*, z_*)$, which is a solution to

$$-\frac{1}{c_0^2} \frac{\partial^2 G}{\partial t^2} + \frac{\partial^2 G}{\partial r^2} + \frac{1}{r} \frac{\partial G}{\partial r} + \frac{\partial^2 G}{\partial z^2} = -\frac{\delta(r - r_*)}{r} \delta(z - z_*) \delta(t - \tau), \tag{2}$$

where δ is Dirac's delta function. It can be shown that the solution is given by

$$G(t, \tau; r, z; r_*, z_*) = \frac{c_0}{\pi} \frac{H(f_n^+) H(f_n^-)}{\sqrt{f_d^+ f_d^-}}, \tag{3}$$

where

$$f_n^+ = r + r_* - \sqrt{c_0^2 (t - \tau)^2 - (z - z_*)^2}, \qquad f_n^- = \sqrt{c_0^2 (t - \tau)^2 - (z - z_*)^2} - |r - r_*|, \tag{4}$$

and

$$f_d^+ = (r+r_*)^2 + (z-z_*)^2 - c_0^2(t-\tau)^2, \qquad f_d^- = c_0^2(t-\tau)^2 - (z-z_*)^2 - (r-r_*)^2. \tag{5}$$

Here $H(f)$ is the Heaviside unit function which takes the value 1 when $f > 0$ and the value 0 when $f < 0$.

By making use of the Green's function, the pressure $p(\mathbf{x}, t)$ at any point $\mathbf{x} = (r, z)$ can be determined as

$$p(t,r,z) = -\rho_0 \int_\tau \left\{ \int_{z_*} \int_{r_*} \nabla_{\mathbf{y}} G \cdot \mathfrak{L} r_* dr_* dz_* + \int_{z_{*1}}^{z_{*2}} \left(p_* \frac{\partial G}{\partial r_*} - G \frac{\partial p_*}{\partial r_*} \right) 2\pi r_* dz_* \right. \tag{6}$$
$$\left. + \int_{r_{*1}}^{r_{*2}} \left(p_* \frac{\partial G}{\partial z_*} - G \frac{\partial p_*}{\partial z_*} \right) 2\pi r_* dr_* \right\} d\tau,$$

where, in the first term, $\nabla_{\mathbf{y}} = (\partial/\partial r_*, \partial/\partial z_*)$. This (first) term represents the 'source' contribution p_s from the vortex rings. The vorticity related to a single ring is given by

$$\boldsymbol{\omega}_j = \Gamma_j \delta(r_* - r_j)\delta(z_* - z_j)\mathbf{i}_\theta, \tag{7}$$

where $\mathbf{i}_\theta$ is a unit vector in the azimuthal direction of the cylindrical polar coordinate system (r, θ, z). Then, by making use of (3, 4), the first term in (6) takes the form

$$p_s = \frac{c_0}{\pi} \rho_0 \sum_j \left\{ \mathrm{sgn}(r, r_j) \frac{\partial}{\partial r} \int_{t-d_j^+/c_0}^{t-d_j^-/c_0} \frac{\Gamma_j(\tau) v_{zj}(\tau)\, r_j}{\sqrt{f_d^+ f_d^-}} d\tau - \mathrm{sgn}(z, z_j) \frac{\partial}{\partial z} \int_{t-d_j^+/c_0}^{t-d_j^-/c_0} \frac{\Gamma_j(\tau) v_{rj}(\tau)\, r_j}{\sqrt{f_d^+ f_d^-}} d\tau \right\}, \tag{8}$$

where the subscript 's' stands for 'source term'. The summation over j refers to summation over all free vortex rings. Note that differentiation with respect to the source variables r_j and z_j have been converted into differentiation with respect to r and z. Here care should be taken with the signs related to r_j and r and to z_j and z; see (4) and (5). This is taken care of by the functions $\mathrm{sgn}(r, r_j)$ and $\mathrm{sgn}(z, z_j)$.

The main contributions to the τ-integrations will be at the end point singularities. Hence the functions f_d^+ and f_d^- can be approximated as

$$f_d^+ \approx 2c_0 d_j^+ \left\{ \tau - (t - d_j^+/c_0) \right\}, \qquad f_d^- \approx 2c_0 d_j^- \left\{ (t - d_j^-/c_0) - \tau \right\}, \tag{9}$$

where

$$d_j^+ = \{(r+r_j)^2 + (z-z_j)^2\}^{\frac{1}{2}}, \qquad d_j^- = \{(r-r_j)^2 + (z-z_j)^2\}^{\frac{1}{2}}. \tag{10}$$

Let $a = t - d_j^+/c_0$ and $b = t - d_j^-/c_0$. The integrals over τ in (8) then take the form

$$I_\tau(t) = \int_a^b \frac{F(\tau)}{\sqrt{(\tau - a)(b - \tau)}}, \tag{11}$$

which is a standard Gauss-Chebyshev integral. The corresponding quadrature formula is given by

$$I_\tau(t) = \sum_{i=1}^{I} w_i F(s_i) + R_I, \qquad s_i = \frac{b+a}{2} + \frac{b-a}{2} t_i, \qquad t_i = \cos\frac{(2i-1)\pi}{2I}, \quad w_i = \frac{\pi}{I}, \tag{12}$$

where R_I is the reminder. Using just one point, i.e. taking $I = 1$, corresponds to assuming that the vortex strengths $\Gamma_j(\tau)$ and the corresponding velocities $v_{rj}(\tau, r_j, z_j)$, $v_{zj}(\tau, r_j, z_j)$ are constant within the limits of integration over τ, and equal to their values at the mean retarded time $\bar{t} = t - (d_j^+ + d_j^-))/2c_0$. Applying this approximation, an evaluation of (8) gives

$$p_s = -\frac{\rho_0}{4}\sum_j \frac{r_j}{\sqrt{d_j^+ d_j^-}}\left[\Gamma_j v_{zj}(\bar{t})\left\{\frac{r+r_j}{(d_j^+)^2} - \frac{r-r_j}{(d_j^-)^2}\right\} + \Gamma_j v_{rj}(\bar{t})(z-z_j)\left\{\frac{1}{(d_j^+)^2} + \frac{1}{(d_j^-)^2}\right\}\right. \quad (13)$$
$$\left. + \frac{1}{c_0}\frac{\partial}{\partial \bar{t}}\left(\Gamma_j v_{zj}(\bar{t})\right)\left\{\frac{r+r_j}{d_j^+} - \frac{r-r_j}{d_j^-}\right\} + \frac{1}{c_0}\frac{\partial}{\partial \bar{t}}\left(\Gamma_j v_{rj}(\bar{t})\right)(z-z_j)\left\{\frac{1}{d_j^+} + \frac{1}{d_j^-}\right\}\right].$$

The second and third terms of (6) make up the scattering contribution p_{sc}, due to the solid surfaces. We use the subscript 'sc' to refer to 'scattered', and the subscript asterisk in p_* to refer to the surface pressure. The second term is for the horizontal sections (integration along the z axis) while the third term is for the vertical surfaces (integration along the r axis). By making use of the same kind of approximations as applied to the vortex source term p_s these terms can be evaluated as

$$p_{sc} = \frac{\pi}{2}\delta_{hc}\int_{z_{*1}}^{z_{*2}} \frac{r_*}{\sqrt{d_*^+ d_*^-}}\left[p_*(\bar{t})\left\{\frac{r+r_*}{(d_*^+)^2} - \frac{r-r_*}{(d_*^-)^2}\right\} + \frac{1}{c_0}\frac{\partial}{\partial \bar{t}}\left(p_*(\bar{t})\right)\left\{\frac{r+r_*}{d_*^+} - \frac{r-r_*}{d_*^-}\right\}\right] dz_* \quad (14)$$
$$-\frac{\pi}{2}\delta_{vc}\int_{r_{*1}}^{r_{*2}} \frac{r_*(z-z_*)}{\sqrt{d_*^+ d_*^-}}\left[p_*(\bar{t})\left\{\frac{1}{(d_*^+)^2} + \frac{1}{(d_*^-)^2}\right\} + \frac{1}{c_0}\frac{\partial}{\partial \bar{t}}\left(p_*(\bar{t})\right)\left\{\frac{1}{d_*^+} + \frac{1}{d_*^-}\right\}\right] dr_*$$
$$+\pi\delta_{ho}\int_{z_{*1}}^{z_{*2}} \frac{r_*}{\sqrt{d_*^+ d_*^-}}\frac{\partial p_*(\bar{t})}{\partial r_*} dz_* + \pi\delta_{vo}\int_{r_{*1}}^{r_{*2}} \frac{r_*}{\sqrt{d_*^+ d_*^-}}\frac{\partial p_*(\bar{t})}{\partial z_*} dr_*.$$

Here δ_{hc} is 1 on horizontal closed (i.e. physical) surfaces, and 0 otherwise; δ_{vc} is 1 on vertical closed surfaces, and 0 otherwise; δ_{ho} is 1 on horizontal open (i.e. virtual, or control) surfaces, and 0 otherwise; and δ_{vo} is 1 on vertical open surfaces, and 0 otherwise.

The total pressure at an observation point (r, z) is now given by

$$\varsigma p(\bar{t}, r, z) = p_s(\bar{t}, r, z) + p_{sc}(\bar{t}, r, z). \quad (15)$$

Here ς is equal to 1 when the observation point is in the acoustic medium and away from the solid boundaries, and equal to $\frac{1}{2}$ when the observation point is located on a solid boundary.

3 Boundary element discretization

Next we employ the boundary element methodology of dividing the surface into V elements, assuming that the pressure is constant within each element. The time dependence of the pressure is, within cosecutive time steps, interpolated via a cubic polynomial. Thus, the pressure anywhere on the boundary $p_*(\bar{t})$ can, at time step W, be expressed as

$$p_*(\bar{t}, r_*, z_*) = \sum_{v=1}^{V}\sum_{w=1}^{W} f_v(r_*, z_*) g_w(\bar{t}) P_{vw}, \quad (16)$$

where

$$f_v(r_*, z_*) = \begin{cases} 1 & \text{for } (r_*, z_*) \in (r_v, z_v) \\ 0 & \text{otherwise} \end{cases}, \quad (17)$$

and $g_w(\bar{t}) = g(t - w\Delta t)$, with

$$g(t) = \begin{cases} 1 + \frac{11}{6}\frac{t}{\Delta t} + \left(\frac{t}{\Delta t}\right)^2 + \frac{1}{6}\left(\frac{t}{\Delta t}\right)^3 & \text{for } -\Delta t \le t < 0, \\ 1 + \frac{1}{2}\frac{t}{\Delta t} - \left(\frac{t}{\Delta t}\right)^2 - \frac{1}{2}\left(\frac{t}{\Delta t}\right)^3 & \text{for } 0 \le t < \Delta t, \\ 1 - \frac{1}{2}\frac{t}{\Delta t} - \left(\frac{t}{\Delta t}\right)^2 + \frac{1}{2}\left(\frac{t}{\Delta t}\right)^3 & \text{for } \Delta t \le t < 2\Delta t, \\ 1 - \frac{11}{6}\frac{t}{\Delta t} + \left(\frac{t}{\Delta t}\right)^2 - \frac{1}{6}\left(\frac{t}{\Delta t}\right)^3 & \text{for } 2\Delta t \le t < 3\Delta t, \\ 0 \quad \text{otherwise.} \end{cases} \tag{18}$$

In the usual collocation type BEM (14) is evaluated at each of the V spatial control points in turn, to give V equations for the V unknown element pressures (at each time step). Here we employ the Galerkin method, where the 'strong form' of these equations are exchanged with a 'weak form'. To this end, (14) is multiplied by the spatial shape function f_u, followed by integration around the closed surface (see also Section 4). Letting u run from 1 to V, we obtain a $V \times V$ equation system on the form

$$\mathbf{A}_0 \mathbf{p}_W = -\sum_{w=1}^{N_{\text{save}}} \mathbf{A}_w \mathbf{p}_{W-w} + \mathbf{f}_W, \tag{19}$$

which is solved at each time step.

4 Boundary element grid and tailpipe representation

The closed surface, which is assumed when applying Green's second identity [7] to convert volume integrals into surface integrals in (6), can be specified in a variety of ways. The standard, and most simple, way would be to represent the solid surfaces by boundary elements, making two separated closed surfaces in the present case, as shown in Fig. 2 (a). This approach has the benefit that the terms proportional to $\partial p_*/\partial r_*$ and $\partial p_*/\partial z_*$ in (14) drop out. But it makes internal resonances possible. This will in turn imply a numerical instability that is difficult to cure. A number of methods to circumvent this problem are available, such as the methods known as CHIEF (Combined Helmholtz Integral Equation Formulation) [10] and CONDOR (Composite Outward Normal Derivative Overlap Relation) [1]. Both of these methods were developed originally for frequency-domain formulations but can be modified to be used in the time domain. Such modifications have been considered for the CONDOR method by [[3]] and [2] and also, very recently, for the CHIEF method by [6].

We have tried to use the latter approach in connection with a grid layout as that shown in Fig. 2 (a) but did not obtain sufficient stabilization. Accordingly, the grid was modified to one as shown in Fig. 2 (b). Here the acoustic medium within the whole hole-tone/pipe system is surrounded by elements; and the resonances that can occur within the closed surface are the *physical* resonances that we are interested in. Yet is was found to be difficult to stabilize the vibrations without damping out the resonance peaks too much. On another note, it can be argued that, since the acoustic waves in the tailpipe principally are one-dimensional, a boundary element representation of this long, slender surface is 'wasteful' from a computational point of view. These considerations, together with the mentioned stability problems, suggest an approach as that shown in Fig. 2 (c).

Here only the hole-tone-system part is represented by boundary elements. The pipe is represented by the exact one-dimensional wave solution, considered as a 'super element', and the two sub-systems are coupled.

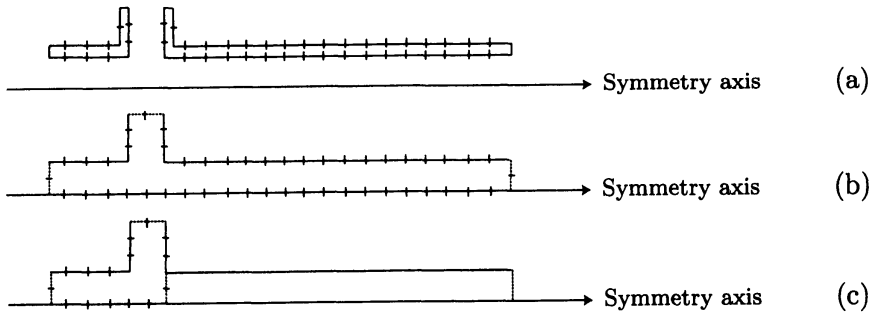

Figure 2: Possible boundary element grids. Dotted lines indicate open (pressure relief) boundaries.

5 Pressure in the tailpipe and acoustic feedback

Let $z = z_1$ correspond to the upstream pipe entrance and $z = z_2$ to the downstream pipe exit. In the following we will use the local coordinate $\tilde{z} = z - z_1$. Also, let $\ell = z_2 - z_1$.

We will assume that the 'driving' disturbance at $\tilde{z} = 0$ can be described in terms of its velocity potential there, ϕ_0 say. Next we will evaluate the velocity potential ϕ in the pipe. Use of the velocity potential is convenient because once it (ϕ) is known the acoustic pressure p and particle velocity can be determined as

$$p = \rho_0 \frac{\partial \phi}{\partial t}, \quad u = -\frac{\partial \phi}{\partial z}. \tag{20}$$

The numerical evaluation of ϕ_0 is based on the pressure gradient at the BEM-pipe interface, $(\partial p/\partial z)_{z=z_1}$.

In the frequency domain, the Green's function corresponding to a disturbance at $\tilde{z} = 0$, of unit amplitude and frequency ω, takes the form

$$\tilde{G}_\phi = \frac{\sin k(\ell - \tilde{z})}{\sin k\ell} \tag{21}$$

where $k = \omega/c_0$. The time-domain version of this equation takes the form

$$G_\phi = \sum_{n=0}^{\infty} \left[\delta\left(t - \frac{\tilde{z} + 2n\ell}{c_0}\right) - \delta\left(t + \frac{\tilde{z} - 2(n+1)\ell}{c_0}\right) \right], \tag{22}$$

where δ is the (Dirac) delta function. Based on this Green's function we get

$$\phi(t, \tilde{z}) = \sum_{n=0}^{\infty} \left[\phi_0\left(t - \frac{\tilde{z} + 2n\ell}{c_0}\right) - \phi_0\left(t + \frac{\tilde{z} - 2(n+1)\ell}{c_0}\right) \right]. \tag{23}$$

In order evaluate the acoustic particle velocity radiated from the pipe it will, for simplicity and as a 'first approximation', be assumed that the one-dimensional velocity field inside the pipe is radiated out in the same one-dimensional way. That is, if z_{1+} is a point a little downstream from the pipe entrance at z_1 the acoustic particle velocity at value of $z < z_1$ is evaluated as

$$u(z, t) = u(z_{1+}, t - (z_{1+} - z)/c_0) \tag{24}$$

The acoustic velocity field is superimposed onto the 'hydrodynamic' velocity field of the free vortex rings in the open domain between nozzle exit and end plate. That is, (24) is evaluated at the position of any free vortex ring in this domain.

6 Numerical examples

In the numerical examples to follow the diameters of nozzle, end plate hole, and tailpipe are all $d_0 = 50\,\text{mm}$. The gap length between nozzle exit and the end plate is also 50 mm. The diameter of the end plate is $3d_0 = 150\,\text{mm}$. The mean jet speed $u_0 = 10\,\text{m/s}$. The (reference) length of the tailpipe attached onto the end plate is $\ell = 21.25d_0 = 1063\,\text{mm}$. The corresponding (reference) pipe resonance frequencies are $f_n = 160\,n$, $n = 1, 2, \cdots$, where even values of n correspond to multiples of a full wavelength.

The time step is chosen as $\Delta t = 1/(10 f_{max})$ where the maximum frequency of interest f_{max} is set to 1100 Hz. The number of boundary elements on a certain 'stretch' of length l_i (between two corners) is set to $N_e = \max[2, \{\text{nint}(4l_i/(c_0\Delta t))\}]$.

Figure 3 shows the appearance and location of free vortex rings in the vicinity of the end plate during one period of oscillation. The fundamental hole-tone frequency $f_0 = 158\,\text{Hz}$, which is about 40 Hz lower than for the case without a tailpipe [8, 9]. The change in f_0 is due to the different flow field that the tailpipe causes.

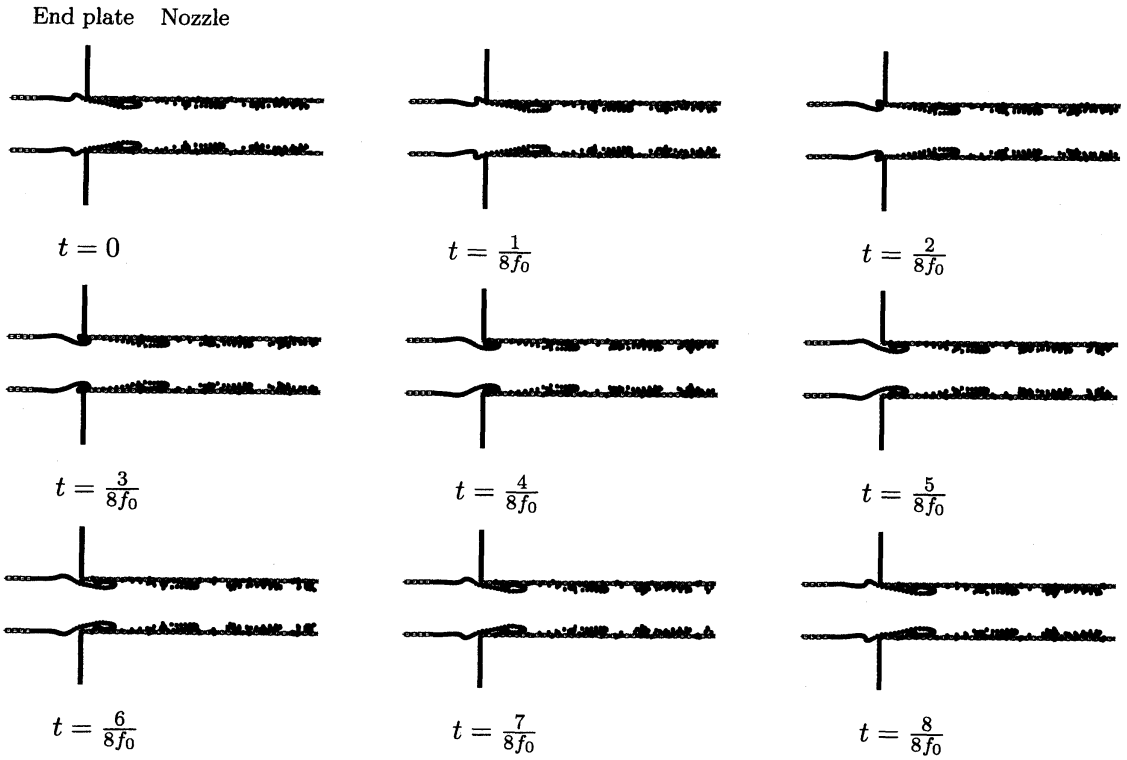

Figure 3: Side view of the vortex rings (in terms of the points $(\pm r_j, z_j)$) during one period of oscillation.

Figure 4 shows a number of time series plots for the pressure variation on the axis of symmetry, in the middle of the tailpipe. It is noted that this position corresponds to a nodal point for the even modes $n = 2, 4, \cdots$. Thus in the corresponding sound pressure spectra (Fig. 5), only the peaks at f_{2n-1}, $n = 1, 2, \cdots$, correspond to pipe resonances; the peaks at f_{2n} correspond to the hole-tone oscillations.

In both of these two figures (4 and 5) the sub-plots on the left-hand side are for cases without acoustic feedback; those on the right-hand side are for cases with acoustic feedback.

In the time series plot of Fig. 4 (a) the hole-tone frequency ($f_0 = 158\,\text{Hz}$) is close to the first (half-wave) eigenfrequency of the pipe pressure oscillations ($f_1 = 160\,\text{Hz}$) but not exactly equal

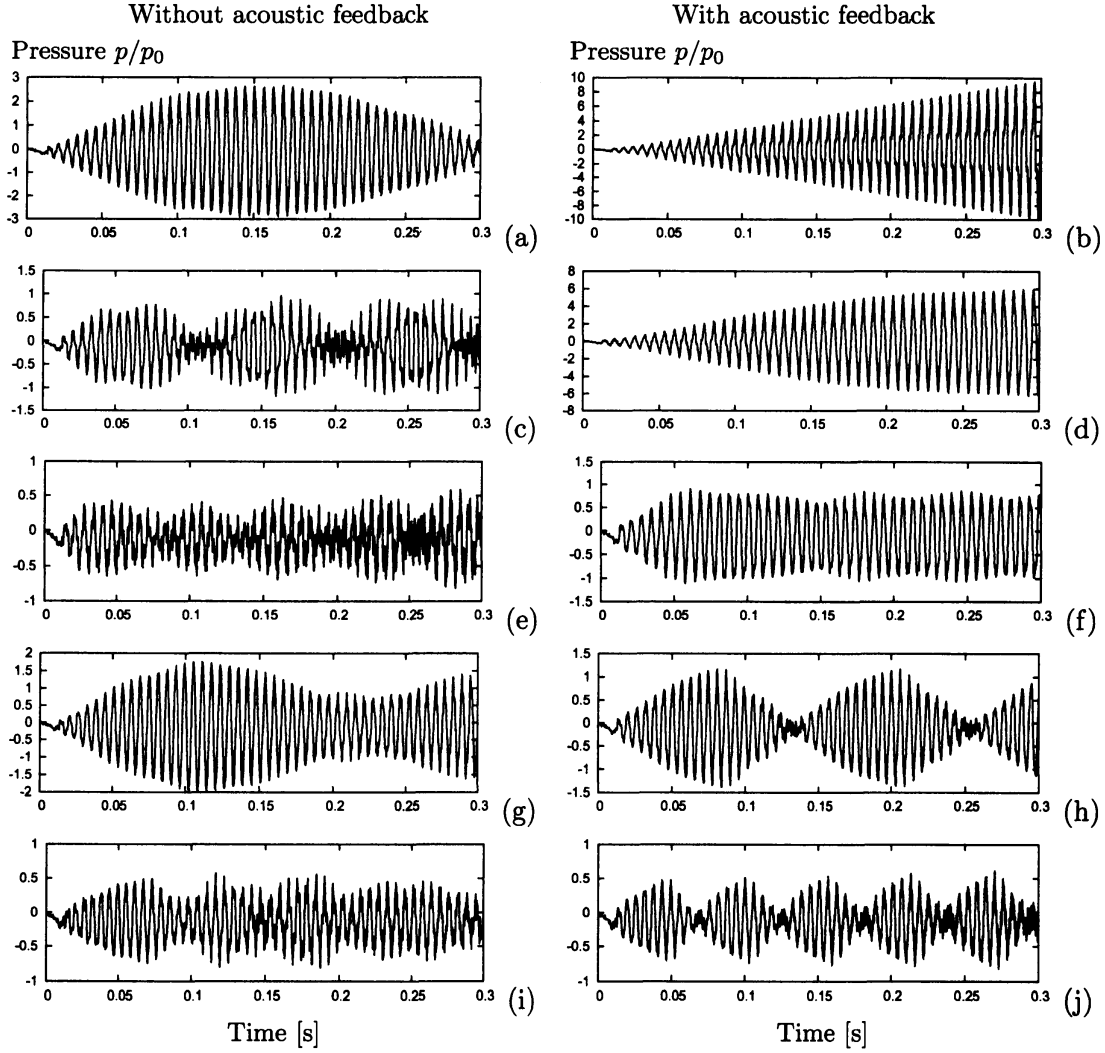

Figure 4: Sound pressure time series. [Reference pressure $p_0 = \frac{1}{2}\rho_0 u_0^2$.] The observation point is on the jet axis, in the middle of the pipe. The sub-plots on the left-hand side are for cases without acoustic feedback; those on the right-hand side are for cases with acoustic feedback. (a, b) Pipe length $\ell = 21.25 d_0$. (c, d) $\ell = 22.25 d_0$. (e, f) $\ell = 23.25 d_0$. (g, h) $\ell = 20.25 d_0$. (i, j) $\ell = 19.25 d_0$.

to it. For this reason a slow beat phenomenon, with a period of 0.5 s, is developed.

When acoustic feedback is included (Fig. 4 (b)) the hole-tone oscillations lock-in to the pipe oscillations, and a clear resonance is developed. The pressure amplitude grows to large values in a almost linear fashion. As a reference, it is noted that the amplitude of a simple, undamped, forced one degree-of-freedom oscillator grows linearly; so the behavior in Fig. 4 (b) appears plausible. Comparing the spectra of Fig. 5 (a) and (b) it is seen that peaks of f_{2n-1} ($n = 1, 2, \cdots$) are raised significantly by the feedback.

The plots in Figs. 4 and 5, parts (c) and (d), are for a pipe of length $\ell = 22.25 d_0$. This gives the resonance frequencies $f_n = 151\, n$, $n = 1, 2, \cdots$. The larger difference between f_0 and f_1 implies faster beats, as seen from Fig. 4 (c). Inclusion of acoustic feedback gives, instead of the beats, again an almost linear pressure amplitude growth (Fig. 4 (d)) - which however 'flattens off' at larger times.

Comparing the spectra in parts (c) and (d) of Fig. 5, it is interesting to note that the peak

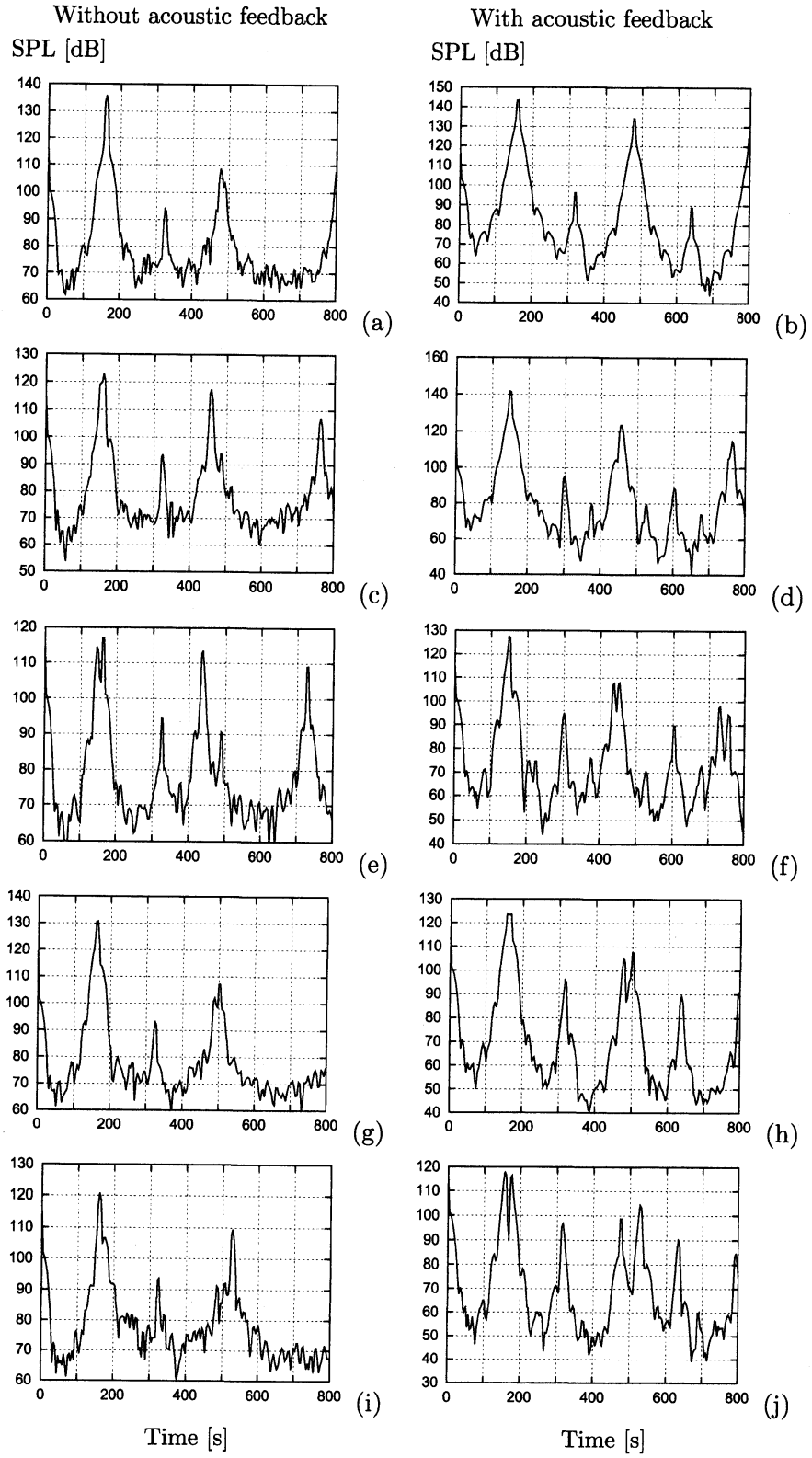

Figure 5: Sound pressure spectra of the time series shown in Fig. 4. [Sound pressure level (SPL) in dB; reference pressure $p_{ref} = 2 \times 10^{-5}$ N/m^2.] Again, the sub-plots on the left-hand side are for cases without acoustic feedback; those on the right-hand side are for cases with acoustic feedback. (a, b) Pipe length $\ell = 21.25 d_0$. (c, d) $\ell = 22.25 d_0$. (e, f) $\ell = 23.25 d_0$. (g, h) $\ell = 20.25 d_0$. (i, j) $\ell = 19.25 d_0$.

at $2f_0 \approx 320\,\mathrm{Hz}$ moves to $2f_0 \approx 300\,\mathrm{Hz} \approx 2f_1$ when acoustic feedback is included. That is to say, the hole-tone frequency f_0 undergoes a lock-in to the pipe resonance frequency f_1.

Figures 4 and 5, parts (e) and (f), show that lock-in of f_0 to f_1 happens also when feedback is included for a pipe a bit longer, of length $\ell = 23.25d_0$, with resonance frequencies $f_n = 146\,n$. Here the pressure amplitude grows linearly only for small values of time t; at larger times it takes an almost-constant value.

Shorter pipes that have resonance frequencies $f_n > f_0$ have been considered as well (Figs. 4 and 5, parts (g)-(j)). But here the acoustic feedback does not easily imply a lock-in of the hole-tone frequency to that of the pipe resonance. More computational studies are needed in order to identify and understand regions (in the parameter space) with lock-in and non-lock-in.

It must be pointed out, lastly, that the magnitude of the feedback velocity field is important, and that one can hardly expect the present simple approach to give the correct magnitude. In the numerical examples presented here, an 'amplification factor' (multiplier) was used to enlarge the numerical value of the velocity. For the pipe lengths $\ell = 19.25d_0$, $20.25d_0$, and $21.25d_0$, the amplification factor was 25; for $\ell = 22.25d_0$ and $23.25d_0$, it was 50.

7 Conclusions

1. Use of a discrete vortex method in combination with the theory of vortex sound and the boundary element method has proved to be an efficient and computationally simple approach for simulation of flow-acoustic interaction problems, like the hole-tone/pipe resonance problem considered here.

2. The employed time-domain boundary element method can be made numerically stable; but (physical, pipe) resonances within the closed boundary domain trigger instability problems. Use of the analytical solution for the acoustic pipe oscillations cures the numerical stability problem. It also reduces the computational costs considerably.

3. The numerical model can display lock-in of the self-sustained flow oscillations to the resonant acoustic oscillations.

Acknowledgement: The work reported here was supported by a Collaborative Research Project Grant (No. J13062) from the Institute of Fluid Science, Tohoku University.

References:

[1] A. J. Burton and G. F. Miller. The application of integral equation methods to the numerical solution of some exterior boundary-value problems. *Proc. Roy. Soc. Lond. (A)*, 323:201–210, 1971.

[2] D. J. Chappell, P. J. Harris, D. Henwood, and R. Chakrabarti. A stable boundary element method for modeling transient acoustic radiation. *J. Acoust. Soc. Am.*, 120:74–80, 2006.

[3] A. A. Ergin, B. Shanker, and E. Michielssen. Analysis of transient wave scattering from rigid bodies using a Burton-Miller approach. *J. Acoust. Soc. Am.*, 106:2396–2404, 1999.

[4] M. S. Howe. *Acoustics of Fluid-Structure Interactions.* Cambridge University Press, 1998.

[5] M. S. Howe. *Theory of Vortex Sound.* Cambridge University Press, 2003.

[6] H.-W. Jang and J.-G. Ih. Stabilization of time domain acoustic boundary element method for the exterior problem avoiding the nonuniqueness. *J. Acoust. Soc. Am.*, 133:1237–1244, 2013.

[7] O. D. Kellogg. *Foundations of Potential Theory.* Dover Publications, New York (1954 republication), 1929.

[8] M. A. Langthjem and M. Nakano. Numerical study of the hole-tone feedback cycle based on an axisymmetric discrete vortex method and Curle's equation. *J. Sound Vibr.*, 288:133–176, 2005.

[9] M. A. Langthjem and M. Nakano. A numerical simulation of the hole-tone feedback cycle based on an axisymmetric formulation. *Fluid Dyn. Res.*, 42:1–26, 2010.

[10] H. A. Schenck. Improved integral formulation for acoustic radiation problems. *J. Acoust. Soc. Am.*, 44:41–58, 1967.